Kinetic Isotope Quantum Effects in the Adsorption of H2O and D2O on Porous Carbons

ARTICLE *in* THE JOURNAL OF PHYSICAL CHEMISTRY C · FEBRUARY 2007

Impact Factor: 4.77 · DOI: 10.1021/jp065105o

2 AUTHORS:

Ashleigh Fletcher
University of Strathclyde
43 PUBLICATIONS **2,921** CITATIONS
SEE PROFILE

Keith Mark Thomas
Newcastle University
198 PUBLICATIONS **10,403** CITATIONS
SEE PROFILE

Kinetic Isotope Quantum Effects in the Adsorption of H_2O and D_2O on Porous Carbons

Ashleigh J. Fletcher and K. Mark Thomas*

Northern Carbon Research Laboratories, School of Natural Sciences, Bedson Building, University of Newcastle upon Tyne, Newcastle upon Tyne, NE1 7RU, U.K.

Received: August 8, 2006; In Final Form: October 26, 2006

This paper describes an investigation of the adsorption characteristics of H_2O and D_2O on two activated carbons, BAX950, containing a range of micro- and mesoporosity, and G209, a predominantly microporous material. Adsorption kinetics of H_2O and D_2O on activated carbon BAX950 were studied over temperature ranges of 293−313 K and 278−303 K, respectively. The adsorption/desorption of H_2O and D_2O were also studied on activated carbon G209 at 298 K. The adsorption isotherms for H_2O and D_2O agree well while greater adsorption hysteresis was observed for H_2O compared with D_2O. Comparison of the adsorption kinetic behavior of H_2O and D_2O indicated a kinetic isotope effect. The trends in isotherm hysteresis, kinetic parameters, and activation energies are attributed to quantum effects, which are the source of differences in intermolecular hydrogen bonding in H_2O and D_2O adsorbates and bonding between these adsorbates and surface oxygen functional groups. The effects of confinement in pores on adsorbate structure are discussed.

1. Introduction

Porous carbon materials have a wide range of applications varying from gas separation and storage, to catalyst supports and adsorption of environmentally unfriendly species from air streams. One of the main problems with assessing the adsorption performance of these materials is the presence of competing species; in particular, in the case of adsorption from air streams, competitive adsorption of water vapor is a problem. Porous carbons have both hydrophobic graphene layers, which are primary sites for adsorption of organic species, and hydrophilic functional groups on which water vapor is initially adsorbed. Previous work has shown that in competitive adsorption of water and organic vapors, water vapor may reduce the adsorption capacity and slow the adsorption kinetics of a system.[1] Therefore, it is necessary to understand the mechanism of water vapor adsorption to understand its effect on competitive adsorption of environmentally unfriendly species.

The mechanism of water vapor adsorption involves initial adsorption on functional groups and the development of clusters of water molecules around these functional groups, which eventually leads to pore filling.[2] D_2O is known to have a different hydrogen bonded structure from H_2O, which is reflected in many thermodynamic properties.[3] This is attributed to differences in the zero-point energy, arising from differences in mass for H_2O and D_2O.[4,5] The effect of deuteration, on physical and chemical properties, depends on many factors. The principal factors for kinetics are the rate-determining step and increased mass, leading to reduced mobility of the heavier deuterated molecule. However, isotopic substitution with a heavier atom sometimes produces a faster rate for the process and this is called an inverse isotope effect, which has been observed in a variety of systems.[6−12]

Recent studies have shown for the first time that kinetic isotope quantum molecular sieving occurs in carbon molecular sieve and porous carbon materials with pore sizes in the range 0.45−0.55 nm with the higher barrier due to the larger zero-point energy for the lighter H_2 resulting in slower adsorption/desorption kinetics compared with the heavier D_2. This is related to quantum effects when the difference in the size of the molecule and the pore is similar to the de Broglie wavelength. The D_2 adsorption and desorption kinetics were significantly faster (up to 1.9×) than the corresponding H_2 kinetics for specific pressure increments/decrements.[13]

In this paper, we report the discovery of a kinetic isotope effect for adsorption of H_2O and D_2O on porous carbons based on differences in adsorbate−adsorbent and adsorbate−adsorbate interactions rather than very small differences in adsorbate and pore sizes as in kinetic isotope quantum molecular sieving. The effect of isotopic substitution on kinetic parameters is discussed in relation to the mechanism of water vapor adsorption and surface chemistry.

2. Experimental

2.1. Materials Used. Carbon BAX950, a wood-based activated carbon, was obtained from the Westvaco Corp. U.S.A. Coconut-shell based activated carbon G209 was manufactured by Usine Pica, Vierzon, France. Both samples have particle size fractions in the range 1−2 mm. The adsorbates used were D_2O (99.9% purity), supplied by Aldrich Chemical Co. Inc, Milwaukee, U.S.A. and high purity water.

2.2. Chemical Analyses. Carbon, hydrogen, nitrogen, and oxygen analyses were carried out by Microanalytical Services, Okehampton, Devon, U.K.

2.3. Functional Group Characterization. *Titration Methods.* Carbon surface amphoteric characteristics were evaluated according to the method of Boehm.[14] A 0.2 g sample of carbon was placed in 25 mL of the following 0.1 N solutions: sodium hydroxide, sodium carbonate, sodium bicarbonate, and hydrochloric acid. The mixtures were equilibrated for 48 h at 298 K before separation by filtering. The excess base and acid were titrated with 0.1 N HCl and 0.1 N NaOH, respectively. The numbers of acidic sites were calculated using the assumption that NaOH neutralizes carboxylic, phenolic, and lactonic groups,

* Author to whom all correspondence should be addressed: E-mail: mark.thomas@ncl.ac.uk.

10.1021/jp065105o CCC: $37.00
Published on Web 01/11/2007

TABLE 1: Porous Structure Characteristics of Carbons Used in This Study

carbon	total pore volume/cm^3 g^{-1}	micropore volume/cm^3 g^{-1}(<2 nm)	micropore volume/cm^3 g^{-1}(<0.7 nm)	average micropore radii/nm
	N_2, 77 K, Langmuir[a]	N_2, 77 K, DR[b]	CO_2, 273 K, DR[b]	Dubinin Stoeckli
BAX950	0.830	0.438	0.152	0.45
G209	0.450	0.345	0.303	0.31

[a] BAX950 has a Type I/II isotherm and the total pore volumes were calculated by extrapolation of the isotherm data at $p/p^0 = 1$. The total pore volume for G209 was determined using the Langmuir equation. [b]Linear part of DR graph was used in micropore volume calculation.

Na_2CO_3 neutralizes carboxylic and lactonic groups, and $NaHCO_3$ neutralizes only carboxylic groups. The number of surface basic sites was calculated from the titer for hydrochloric acid.

Temperature Programmed Desorption (TPD). TPD studies were carried out using a Thermal Science STA 1500 thermogravimetric analyzer (TGA) connected to a VG Quadrupole 300 amu mass spectrometer by a heated stainless steel capillary, lined with deactivated fused silica. Five milligrams of carbon was placed in a sample bucket and heated from ambient temperature to 1373 K (heating rate 15 K min^{-1}) under flowing argon (50 mL min^{-1}). Evolved gases were sampled ~5 mm from the surface of the sample and analyzed by quadrupole mass spectrometry throughout the desorption process. Mass to charge (m/z) values of 28 and 44 were monitored, corresponding to evolution of CO and CO_2, respectively, for analysis of surface functional groups.

2.4. Adsorption Studies. An Intelligent Gravimetric Analyzer (IGA) supplied by Hiden Isochema Ltd., Warrington, U.K., was used in this study. This instrument is an ultrahigh vacuum clean system with diaphragm and turbo pumps. The apparatus was used to determine adsorption isotherms for H_2O, D_2O, carbon dioxide (273 K), and nitrogen (77 K). The corresponding kinetics of adsorption and desorption were determined for set pressure steps.[15] The balance and pressure control systems were controlled thermostatically to ± 0.1 K to eliminate changes in the external environment. The microbalance had a long-term stability of 1 μg with a weighing resolution of 0.2 μg. The carbon sample 100 (±1) mg was outgassed to a constant weight at a pressure of $<10^{-6}$ Pa at 473 K. In the case of H_2O and D_2O adsorption, the liquid used to generate the vapor was degassed fully by repeated evacuation and vapor equilibration cycles of the liquid supply side of the vapor reservoir. Typically, >50 cycles were used to degas the liquid. The first isotherm measured after degassing the liquid was regarded as a system purge run to ensure that all the gas in the liquid was removed. In the case of D_2O adsorption, the first isotherm, which took 3−4 days, was repeated to ensure that any deuterium isotope exchange with surface functional groups had fully equilibrated by exposure to D_2O for ~7 days. The vapor or gas pressure was gradually increased over a time scale of ~30 s to prevent disruption of the microbalance until the desired value was achieved. Pressure control was achieved via the use of three transducers with ranges of 0−0.2, 0−10, and 0−100 kPa, each with an accuracy of 0.02% of the specified range. The pressure was maintained at the set point by active computer control of the inlet/outlet valves throughout the duration of the experiment. Pressure steps in the ranges of p/p^0 values 0−0.97 and 0−0.85 were used to obtain the isotherms for D_2O and H_2O, respectively. Buoyancy corrections were performed for all components on the sample and counterweight sides of the balance. The mass uptake was measured as a function of time and the approach to equilibrium monitored in real time with a computer algorithm. After equilibrium was established, the vapor pressure was increased to the next set pressure value and the subsequent uptake was measured until equilibrium was reestablished. The increase in weight due to adsorption for each pressure step was used to calculate the kinetic parameters for adsorption using an appropriate kinetic model. The errors in the calculated rate constants were typically better than ±2%. The sample temperature was monitored throughout the experiment and the variation in sample temperature was minimal (<0.1 K). In the case of desorption, the reverse procedure was carried out. The adsorption isotherms for H_2O and D_2O for various temperatures were carried out in steps of relative pressure, thereby corresponding to steps of surface coverage. The saturated vapor pressures were calculated using the following equation:[16]

$$\log p^0 = A - \frac{B}{T + C} \tag{1}$$

where p^0 is the saturated vapor pressure (Torr), T is the temperature (°C) and A, B, and C are constants defined by the adsorbate. The constants used were: water (263−373 K), (A) 8.09553, (B) 1747.32, (C) 235.074; deuterium oxide (273−333 K), (A) 8.14371, (B) 1746.15, (C) 230.59; carbon dioxide (77−303 K), (A) 7.81024, (B) 995.705, (C) 293.475; and nitrogen (75−125 K), (A) 6.49457, (B) 255.68, (C) 266.550.

TABLE 2: Pore Size Distribution Contributions from Total, <2 and <0.7 nm Pore Volumes

carbon	pore volume distribution, %		
	<0.7 nm	0.7−2.0 nm	>2.0 nm
BAX950	16.8	31.6	51.6
G209	80.0	11.0	9.0

3. Results

3.1. Porous Structure Characteristics of Adsorbents Used in This Study. The porous structures of carbons BAX950 and G209 were characterized using nitrogen adsorption at 77 K and carbon dioxide adsorption at 273 K and the data are given in Tables 1 and 2. The micropore volumes of the carbons were obtained using the Dubinin−Radushkevich (DR) equation, which is as follows:

$$\log n = \log n_0 - D \log^2(p^0/p) \tag{2}$$

where n is the amount adsorbed, n_0 is the amount adsorbed corresponding to the micropore volume, p is the pressure, p^0 is the saturated vapor pressure, and D is a constant related to the microporous structure of the adsorbent.[17] Extrapolation of the DR equation to $p/p^0 = 1$ for carbon dioxide (273 K) and nitrogen (77 K) adsorption data, gives micropore volumes for pore sizes <~0.7 and <2 nm, respectively.[18−20] Total pore volumes were obtained from nitrogen uptakes at $p/p^0 = 1$ and 77 K. The total and micropore volumes were calculated assuming adsorbate densities of 1.023 g cm^{-3} and 0.8081 g cm^{-3} for carbon dioxide and nitrogen, respectively.

Comparison of the data show that G209 is almost exclusively a microporous material with ~80% of the pores <0.7 nm while BAX950 has a mixture of meso- and micropores. The pore size distribution based on size ranges <0.7, 0.7−2, and >2 nm are shown in Table 2. The pore size distributions obtained for

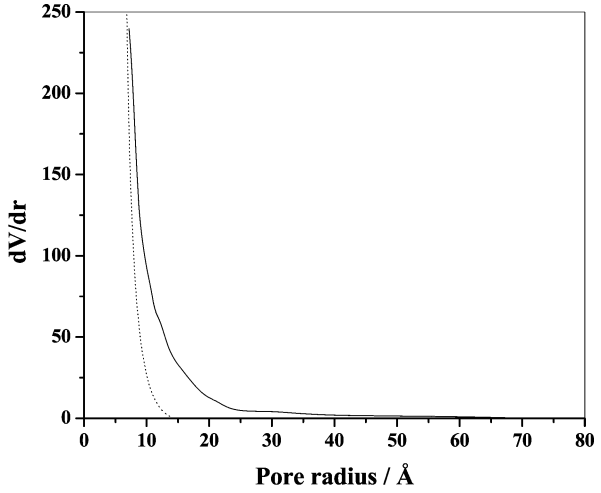

Figure 1. Pore size distributions for G209 (----) and BAX950 (——) determined from BJH analysis of nitrogen adsorption at 77 K.

TABLE 3: Analytical Data(wt % daf Basis) for the Carbons Used in This Study

carbon	C	H	N	O	O/C × 100[a]
G209	96.22	0.42	0.28	2.95	2.29
BAX950	90.67	1.82	0.29	8.72	7.21

[a] Atomic ratio.

BAX950 and G209 from the nitrogen adsorption data at 77 K, using the method of Barrett, Joyner and Halenda (BJH),[21] are shown in Figure 1. These distributions show that the maximum pore size is ~2 nm in G209 and ~6 nm in BAX950. The method establishes the absence of larger mesopores but the use of the method for characterization of pore sizes in the micropore and lower end of mesopore ranges is questionable. Therefore, the micropore volume data were used to show differences between porous structures. The average pore radius of G209, obtained by the method of Dubinin and Stoeckli,[22] was 0.31 nm. The corresponding value for BAX950 was 0.45 nm; however, this value must be considered with caution because of the wide pore size distribution of the material.

3.2. Functional Group Characterization. *Elemental Analysis.* The analytical data for the carbons used in this study are given in Table 3. The oxygen contents were 2.95 and 8.72 wt % daf for G209 and BAX950, respectively. The O/C atomic ratio is ~3× larger for BAX950 than for G209. The nitrogen contents for both carbons were <0.3 wt %; therefore, nitrogen functional groups have negligible influence on adsorption characteristics in these materials.

Titration Studies. Carbon materials contain a mixture of functional groups and have amphoteric surface characteristics. The titration method of Boehm provides a semiquantitative method for functional group characterization and the results showed that G209 was a basic carbon that neutralizes 0.61 meq g^{-1} of HCl. This indicates the presence of mainly chromene and pyrone oxygen functional groups. BAX950 was weakly acidic neutralizing 2.09 meq g^{-1} of NaOH. Titration with $NaHCO_3$ and Na_2CO_3 showed that BAX950 had a high proportion of phenolic (~78%) with a small amount of carboxylic acid groups also present on the surface.

TPD. TPD profiles can be used to establish the total amounts of CO and CO_2 evolved quantitatively and to identify functional groups in a semiquantitative manner.[23] TPD studies (see Supporting Information) showed that functional group desorption started at ~750 K with main peaks observed for BAX950 at 933 and 1253 K for CO and at 978 and 1236 K for CO_2. The

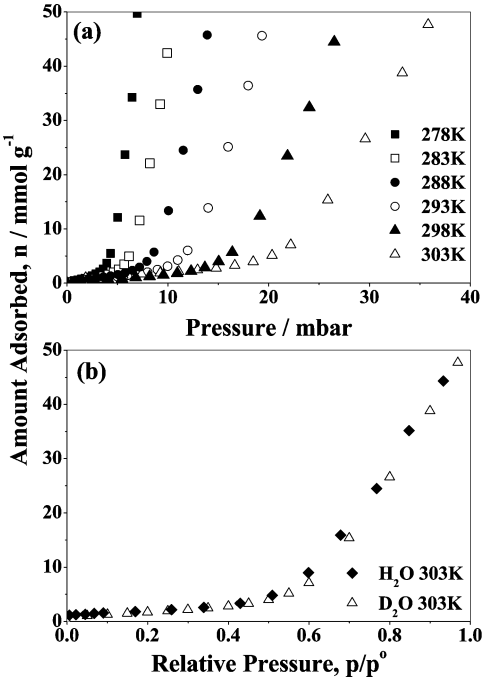

Figure 2. Isotherms for (a) D_2O adsorption on activated carbon BAX950 on a pressure basis for temperature range 278−303 K and (b) comparison of H_2O and D_2O adsorption on activated carbon BAX950 at 303 K on a relative pressure basis.

TPD profiles for G209 had broad peaks for CO at 680, 905, and 1113 K with peaks for CO_2 at 670 and 1180 K. The total integrated CO_2/CO ratios were 0.495 and 0.095 for BAX950 and G209, respectively. Comparison of these data with previous reported CO_2/CO ratios shows that they are consistent with BAX950 being an acidic carbon and G209 being a basic carbon. This is consistent with the titration data.[23]

3.3. Adsorption Isotherm Measurements. Isotherms for the adsorption of D_2O vapor on activated carbon BAX950 over the temperature range 278−303 K are shown in Figure 2a on an absolute pressure basis. H_2O adsorption isotherm data for the temperature range 293−313 K agree well with those for D_2O. The limited temperature range overlap of the data is due to the very long equilibration times for water vapor adsorption below 293 K, due to slow adsorption kinetics, which make further measurements impractical. A typical comparison of D_2O and H_2O adsorption isotherms for BAX950 at 303 K is shown in Figure 2b. Adsorption isotherms obtained for both H_2O[24] and D_2O vapors are classified as Type III in the IUPAC classification scheme.[25] Isotherms for the adsorption/desorption of H_2O and D_2O on activated carbon G209 on a relative pressure basis at 298 K are shown in Figure 3. The adsorption isotherms are classified as Type V in the IUPAC classification scheme.[25] Both BAX950 and G209 have small uptakes at low relative pressures with a sharp increase at $p/p^0 > 0.5$. The difference between the isotherms for BAX950 and G209 is that the latter has a plateau at high relative pressure whereas the former does not. This difference is due to the wider pore size distribution in BAX950 compared with G209. These isotherm characteristics are indicative of systems in which the adsorbate−adsorbate interactions at low relative pressures are stronger than adsorbate−adsorbent interactions.

Comparison of the two sets of adsorption/desorption data for adsorption on G209 shows that the two systems exhibit a significant amount of hysteresis. Kinetic profiles, which show that a true equilibrium has been reached during desorption, are given in Supporting Information. The hysteresis is greater for

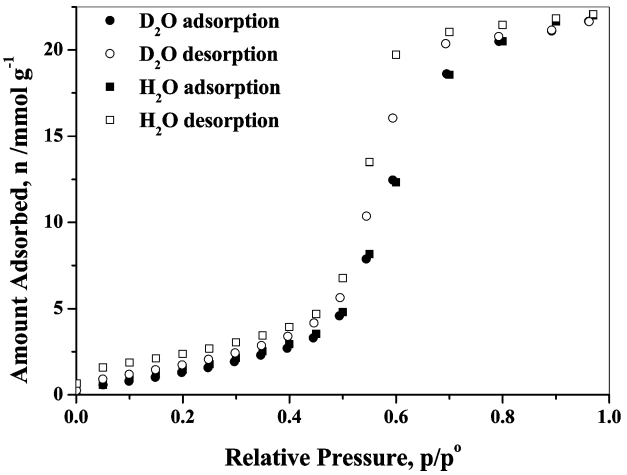

Figure 3. Isotherms for adsorption and desorption of H_2O and D_2O on activated carbon G209 at 298 K.

H_2O adsorption/desorption on G209 (average ~33%) compared to D_2O (average ~24%) over p/p^0 range of 0.5−0.7. This is attributed to differences in the H_2O and D_2O adsorbed phase structures.

3.4. Adsorption Kinetics. This study focuses on the adsorption kinetics of H_2O and D_2O on activated carbon BAX950. D will exchange with O—H or N—H but not C—H[26], and there is the possibility of isotopic exchange between D from the adsorptive (D_2O) and H from carbon surface functional groups. An outgassed sample of activated carbon BAX950 was equilibrated in D_2O prior to adsorption studies and temperature programmed desorption showed a small amount of exchange occurred between surface groups and D_2O (see Supporting Information). Therefore, throughout this study the carbon samples were equilibrated with D_2O prior to the commencement of the D_2O adsorption studies.

A linear driving force mass transfer model (LDF) can be used to describe the adsorption kinetics of a system where the rate-determining step is the existence of a barrier to diffusion.[27−31] The model is described by the equation

$$\frac{M_t}{M_e} = 1 - e^{-kt} \tag{3}$$

where M_t is the uptake at time t, M_e is the equilibrium uptake, and k is the rate constant. The LDF model is a nested kinetic model of the stretched exponential (SE) model. The SE model is described by the following equation

$$\frac{M_t}{M_e} = 1 - e^{-(kt)^\beta} \tag{4}$$

where the parameters are as defined in eq 3, and β is the exponential parameter of the adsorption process. The SE model has been used to describe the adsorption of H_2 and D_2 on carbon molecular sieves and ultramicroporous carbons.[13]

The exponent β covers the range $0 < \beta < 1$ and represents a hierarchy of waiting times for defects hopping in a random environment.[32] The derivation of the stretched exponential decay law for different physical mechanisms has an underlying common mathematical structure.[33] The SE model is one-dimensional with a distribution of relaxation times when $\beta = 0.5$, and three-dimensional (3D) with a single relaxation time when $\beta = 1$. This suggests that intermediate values of β correspond to transitional states and may describe two-dimensional processes.

The kinetics of D_2O adsorption on activated carbon BAX950 follow a stretched exponential model for $p/p^0 = 0-0.97$. A typical normalized profile is shown in Figure 4a together with the residuals from fitting the SE kinetic model to the data. The residuals have all of the profile within ± 0.01, and the SE model fits the experimental data with a high degree of accuracy. A typical normalized profile for H_2O adsorption on BAX950, the corresponding fit for the SE model, and the residuals are shown in Figure 4b. It is evident that the SE model can be used to analyze both the H_2O and D_2O adsorption kinetic data for BAX950.

Figures 5a and b show the SE rate constants and exponents (β) for adsorption of D_2O in the relative pressure range $p/p^0 = 0-0.97$ over the temperature range 278−303 K. The rate constants for adsorption decrease with increasing surface coverage. The SE exponent β varies from 0.50−0.63 at low relative pressure to approximately 0.85−1 above $p/p^0 \sim 0.7$ depending on the temperature. When $\beta = 1$, the SE model becomes the LDF model, which is a nested model of the SE model.

Analysis of the data obtained for adsorption of water on activated carbon BAX950 obtained over the temperature range 293−313 K using the stretched exponential model shows a trend of decreasing rate constant with increasing relative pressure similar to that obtained using the LDF model as shown in Figure 6.[24,34] However, the errors associated with the rate constants obtained from the stretched exponential model are reduced markedly, as might be expected from the inclusion of an additional variable. The trend in exponent β for H_2O adsorption also shows an increase from $\beta \sim 0.5-0.65$ at low relative pressure to $\beta \sim 1$ at high relative pressures ($p/p^0 > 0.6$). The trends obtained for the rate constant and exponent β for D_2O adsorption are similar to those for H_2O adsorption on activated carbon BAX950. Therefore, the rate constants obtained for D_2O at a specific temperature and relative pressure can be compared with H_2O under the same conditions.

The temperature ranges for H_2O and D_2O adsorption isotherms for BAX950 overlap for 293−303 K. Figure 7 shows a comparison of the kinetic parameters for H_2O and D_2O adsorption for 293 and 303 K, which are the extremes of the overlap region. It is evident that D_2O adsorption is faster than H_2O adsorption for $p/p^0 < 0.5$. In the higher pressure range of $p/p^0 > 0.6$, the kinetic parameters are quite similar for 293 and 303 K.

The kinetic data for adsorption of H_2O and D_2O on activated carbon G209 at 298 K also obeyed the stretched exponential model for $p/p^0 = 0-0.97$. The rate constant data obtained for H_2O and D_2O adsorption on activated carbon G209 are shown in Figure 8. It is evident that the rate constant initially decreases with increasing relative pressure. The SE exponent (β) for adsorption, increases from ~0.6 at low loading (i.e., low relative pressure) to ~1 at $p/p^0 > 0.5$ (see Supporting Information). Similar trends in H_2O and D_2O rate constant parameters are observed for $p/p^0 < \sim 0.5$ with D_2O being faster than H_2O. In contrast, the kinetic parameters for H_2O adsorption are slightly faster than D_2O for $p/p^0 > 0.7$ (i.e., on the isotherm plateau).

BAX950 and G209 have acidic and basic characteristics, respectively, and also have markedly different pore size distributions. However, there are similarities between the adsorption kinetic behavior for H_2O and D_2O for G209 and BAX950 in the low relative pressure range of the isotherm. Therefore, differences in functional group composition and pore size distribution do not influence the kinetic trends markedly. Small differences in trends in kinetic parameters are observed

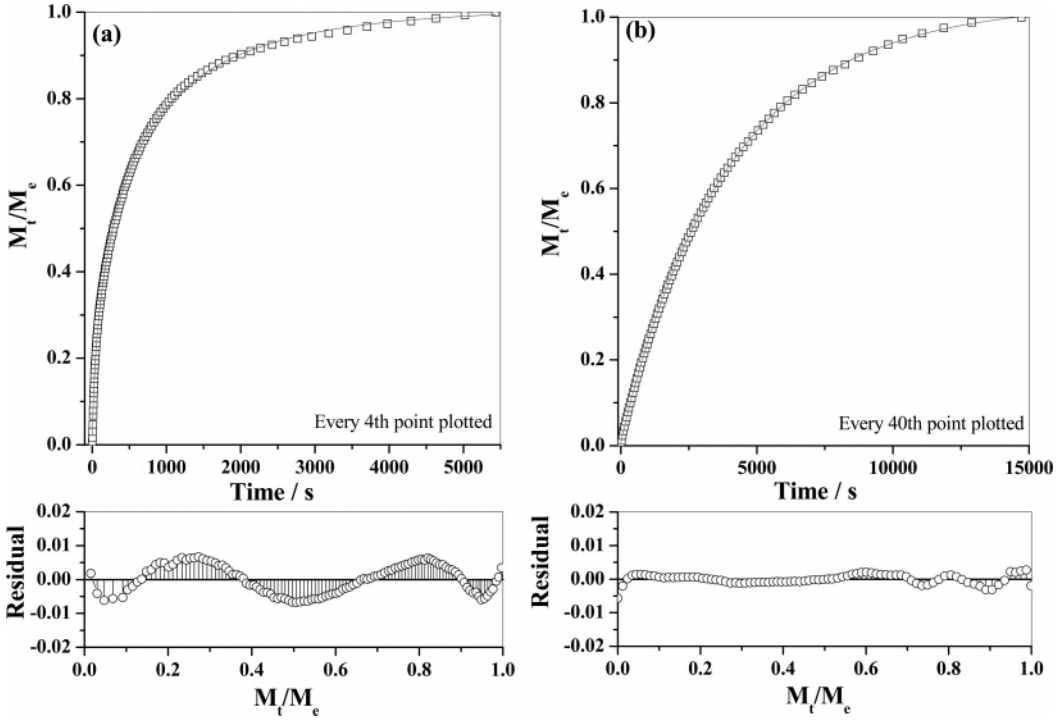

Figure 4. Adsorption kinetic profiles and corresponding fit to the stretched exponential model for (a) D_2O on activated carbon BAX950 at 293 K, $p/p^0 = 0.3997-0.4498$ (0.798−0.898 kPa) and (b) H_2O on activated carbon BAX950 at 293K, $p/p^0 = 0.6876-0.7866$ (1.897−2.170 kPa).

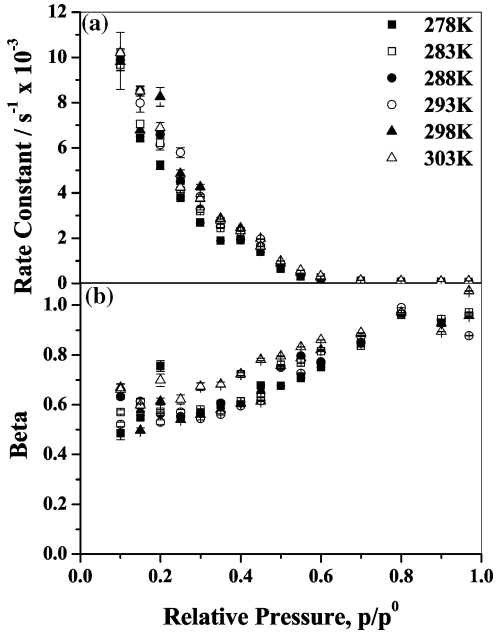

Figure 5. Variation in rate constant with relative pressure for D_2O adsorption on activated carbon BAX950 over the temperature range 278−303 K. (a) SE rate constant and (b) SE β exponent value.

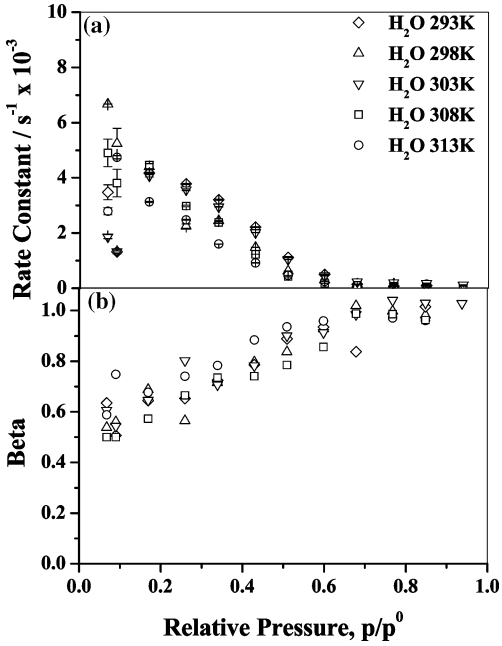

Figure 6. Variation in stretched exponential kinetic parameters with relative pressure for H_2O adsorption on activated carbon BAX950 in the temperature range 293−313 K. (a) SE rate constant and (b) SE β exponent value.

at high relative pressure in which G209 reaches a plateau, whereas BAX950 increases until pore filling occurs at $p/p^0 = 1$.

4. Discussion

4.1. Adsorption Isotherms. Adsorption/desorption of H_2O and D_2O showed that the adsorption isotherms were very similar but more pronounced hysteresis was observed for H_2O compared with D_2O for both activated carbons. This is attributed to differences in the structures of the adsorbates.

The pore volumes, calculated from the uptake estimate for $p/p^0 = 1$, for H_2O and D_2O adsorption on BAX950 were 0.774 and 0.766 $cm^3\ g^{-1}$, respectively. These values are lower than those obtained for *n*-octane (0.85 $cm^3\ g^{-1}$),[35] *n*-nonane (0.89 $cm^3\ g^{-1}$),[35] methanol, ethanol, butan-1-ol and propan-1-ol (0.84 $cm^3\ g^{-1}$),[34] and nitrogen adsorption at 77 K (0.83 $cm^3\ g^{-1}$).[24,34] The pore volume obtained for H_2O adsorption on G209 was 0.396 $cm^3\ g^{-1}$, which is similar to the pore volume (0.391 $cm^3\ g^{-1}$) obtained for adsorption of D_2O. These values are also slightly lower than the total pore volume of 0.450 $cm^3\ g^{-1}$ obtained from nitrogen adsorption at 77 K. The pore volumes derived from H_2O and D_2O adsorption are very similar and are consistent with the molar volume of D_2O being 0.12% higher

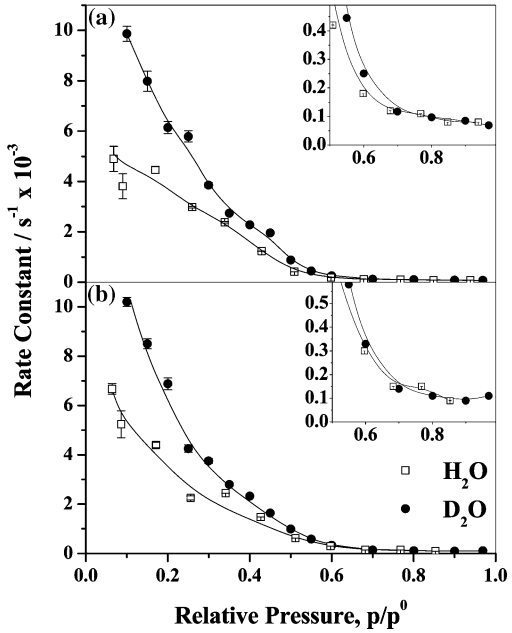

Figure 7. Variation in stretched exponential kinetic parameters with relative pressure for adsorption/desorption of H_2O and D_2O on activated carbon BAX950. (a) 293 K and (b) 303 K.

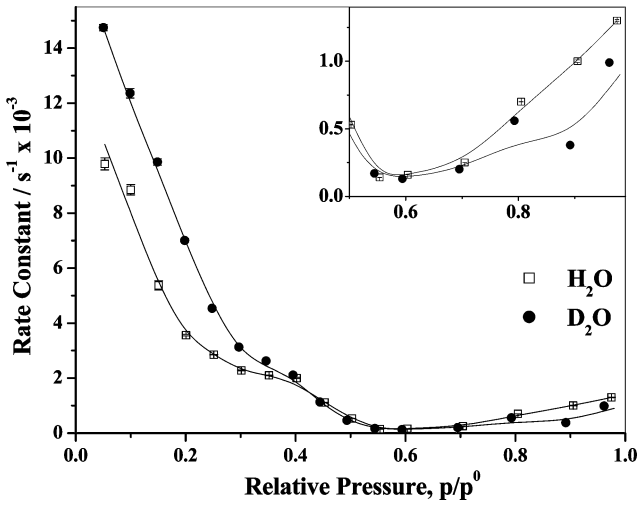

Figure 8. Variation in SE rate constant with relative pressure for adsorption of H_2O and D_2O on activated carbon G209 at 298 K.

than H_2O. The lower pore volume obtained for the adsorption of H_2O on microporous carbons compared with the total pore volumes has been ascribed to a lower adsorbate density than bulk H_2O.[28,36−39]

4.2. Adsorption Activation Energies. Figure 9 shows the variation of activation energy with p/p^0 for H_2O and D_2O adsorption on activated carbon BAX950. The Arrhenius graphs for the adsorption of H_2O and D_2O on BAX950 are given in Supporting Information. The activation energies for H_2O adsorption are consistently higher than the corresponding values for D_2O up to $p/p^0 = 0.85$ (uptake ~30 mmol g^{-1}). However, the higher values for H_2O adsorption are <3 standard deviations different from the corresponding D_2O values for $p/p^0 < 0.3$ (uptake <2 mmol g^{-1}). The activation energies for H_2O and D_2O adsorption increase slightly with increasing relative pressure up to $p/p^0 \sim 0.3$ (2 mmol g^{-1}). A plateau is observed for D_2O activation energies over the relative pressure range of 0.3−0.8, corresponding to uptakes in the range of 2−30 mmol g^{-1}. All the activation energies for D_2O adsorption were <17 kJ mol^{-1}. The graphs of activation energy versus p/p^0 for H_2O

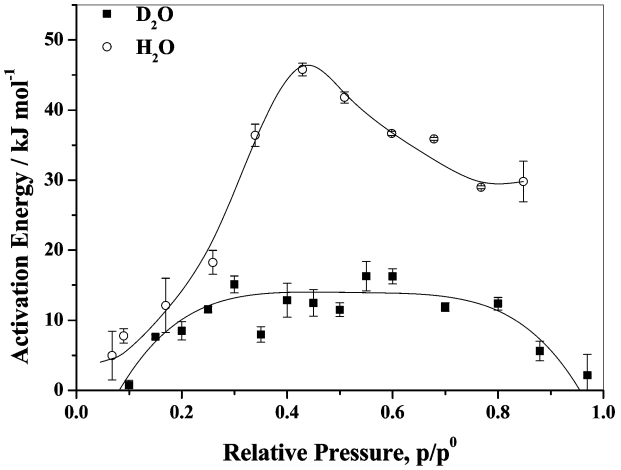

Figure 9. Variation in activation energy with relative pressure (p/p^0) for H_2O and D_2O adsorption on activated carbon BAX950.

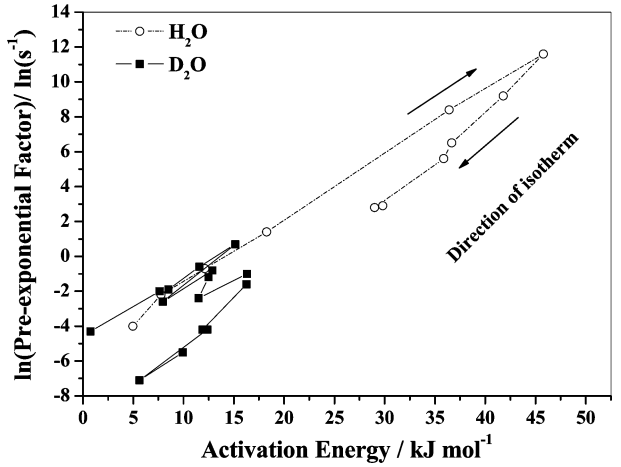

Figure 10. The variation of activation energy with pre-exponential factor for H_2O and D_2O adsorption on activated carbon BAX950.

and D_2O show a marked difference with a well-defined peak for H_2O adsorption observed at $p/p^0 \sim 0.43$, corresponding to an uptake of 4.8 mmol g^{-1}. This peak is in the region of the isotherm in which clusters develop around functional groups. The activation energy peak (45.8 ± 0.9 kJ mol^{-1}) for H_2O adsorption is much greater than the corresponding value for D_2O (11.5 ± 1.0 kJ mol^{-1}), while the activation energies for the D_2O plateau for p/p^0 range 0.3−0.8 averaged 12.45 ± 2.35 kJ mol^{-1}. The results indicate that there are much larger barriers to diffusion of H_2O into the porous structure compared with D_2O adsorption for $p/p^0 > 0.3$.

The activation energies for both H_2O and D_2O adsorption are <50 kJ mol^{-1}. Similar values have been obtained previously for separate investigations with partially associative adsorption of methanol,[34] ethanol,[34] and butan-1-ol,[34] and nonassociative adsorption of *n*-octane[35] and *n*-nonane[35] on activated carbon BAX950, and also for the diffusion of oxygen, nitrogen, argon, etc. on carbon molecular sieves.[27−31]

The variation of activation energy with pre-exponential factor for H_2O and D_2O adsorption on BAX950 is shown in Figure 10. It is apparent that there is a linear correlation for H_2O adsorption. The data obtained exhibit a "true" compensation effect[34] having non-zero isokinetic rates. H_2O has a point in which the gradient changes with respect to isotherm direction (Figure 10) and this is associated with the formation of H_2O clusters around functional groups. Recent studies of adsorption kinetics of gases and vapors, ranging from hydrophobic to

hydrophilic in character, on activated carbons and porous metal organic framework materials have shown that the Arrhenius parameters obtained often show a compensation effect. The data obtained agree well with those from previous studies[24,34,35,40,41] suggesting that the effect is a general one independent of adsorbent or adsorbate characteristics. The corresponding data for D_2O adsorption on BAX950 have a small range of activation energies and are grouped closely together overlapping the H_2O data.

4.3. Molecular Transport in Porous Materials. Diffusion of H_2O and D_2O into porous materials may involve surface, Knudsen, and gas-phase diffusion depending on the mean free path of the species relative to pore widths. The mean free paths (λ_{mfp}) were calculated, using data on collision diameters,[42] from the equation

$$\lambda_{mfp} = \frac{RT}{\sqrt{2}\pi d^2 N_A P} \quad (5)$$

where P is the pressure, T is the temperature in Kelvin, R is the gas constant, d is the collision diameter, and N_A is Avogadro's constant. The minimum values of λ_{mfp} for the systems used in this study occur for the highest pressure studied, which is at the highest temperature (313 K). These calculations, using 0.252 nm as a collision diameter for both H_2O[42] and D_2O, gave minimum values for λ_{mfp} of $\sim$2 μm for both H_2O and D_2O adsorption. BAX950 and G209 have maximum pore widths of $\sim$6 and $\sim$2 nm, respectively, indicating that only surface diffusion needs to be considered.

Adsorption of H_2 and D_2 (dimensions 240 $\times$ 240 $\times$ 310 pm) on porous carbon materials occurs via a nonassociative mechanism, and considering the mass and larger adsorbate−adsorbent interaction of D_2 compared with H_2, one might initially expect that D_2 adsorption kinetics would be slower than H_2 under the same experimental conditions. However, kinetic measurements for H_2 and D_2 adsorption on a carbon molecular sieve and an ultramicroporous carbon at 77 K showed that D_2 adsorption was faster than H_2 adsorption.[13] This was attributed to quantum effects when the adsorbate molecule and pore sizes are similar and their difference is close to the de Broglie wavelength (λ_{DB}). Confinement of the quantum fluid reduces the diffusivity compared to the bulk fluid in which diffusivity increases due to tunneling. The decrease in the well depth for H_2 compared to D_2 increases the hardness of the adsorbate−adsorbent interaction and increases the effective size parameter. The latter was the major factor in determining the kinetic differences.[43,44]

The adsorption of H_2O and D_2O involves an associative mechanism and is more complex than the nonassociative adsorption of H_2 and D_2. The de Broglie wavelengths for H_2O and D_2O, which have dimensions of 291.7 $\times$ 322.6 $\times$ 388.8 pm as determined by Zerner's intermediate neglect of differential overlap (ZINDO) calculations,[45] do not vary markedly over the temperature range studied. These wavelengths are very small ($\sim$40 pm) at 293 K and are similar because of the small difference in mass. These values for λ_{DB} and the pore size distributions of the materials suggest that quantum molecular sieving effects for H_2O and D_2O vapor adsorption, which are similar to H_2 and D_2, at most are small.

H_2O and D_2O have different physical properties due to quantum effects, and studies using rigid-body centroid molecular dynamics methods have shown that quantum effects have a significant influence on equilibrium and dynamical properties of H_2O and D_2O bulk liquids.[46−49] Quantum D_2O has stronger intermolecular bonds than quantum H_2O in the liquid phase. This is consistent with assuming that H-bond strength can be approximated by half the enthalpy of evaporation where the results available for temperatures >323 K show that D_2O has stronger intermolecular bonds than H_2O.[50] The principal intermolecular forces in H_2O (H-bond interactions) are very directional but in a quantum system the forces are averaged over the molecular rotational uncertainty. More than 90% of the quantum effect in H_2O comes from rotational uncertainty because the water molecule has small moments of inertia relative to its large mass and there is a larger effect of quantization for H_2O than D_2O.

Low Relative Pressure ($p/p^0 < 0.4$)/Low Surface Coverage. At low surface coverage, adsorption of H_2O occurs mainly by hydrogen bonding to oxygen surface functional groups. The adsorption kinetics for H_2O and D_2O are influenced by two main factors: (a) the strength of the interaction with the surface functional groups and (b) the barriers to diffusion into the porous structure. The kinetic parameters for D_2O adsorption (kD_2O) are faster than the corresponding parameters for H_2O adsorption (kH_2O) for $p/p^0 < \sim$0.5, for both BAX950 and G209 when compared on a p/p^0 basis, which corresponds to an amount adsorbed basis, because the isotherms overlap closely. At 298 K, the vapor pressure of D_2O is 86% that of H_2O. When the kinetic parameters are plotted on an absolute pressure basis, it brings the kinetic parameters closer together but they do not overlap (see Supporting Information). The SE exponent (β) values obtained for all adsorption systems studied are in the range $\sim$0.5−0.65 at low relative pressure and low loading. This is consistent with a distribution of relaxation times and reflects surface heterogeneity. BAX950 and G209 have oxygen contents of 8.72 wt % and 2.95 wt %, respectively, which correspond to 5.45 and 1.84 mmol g^{-1} of oxygen atoms in the carbons, respectively. The amounts of water adsorbed, which correspond to these values for BAX950 and G209, occur at $p/p^\circ = 0.52$ and 0.27, respectively.

The observation that D_2O adsorption is faster than H_2O adsorption for both acidic BAX950 and basic G209 carbons indicates that the type of surface functional groups is not a major factor. The activation energies for H_2O adsorption are consistently higher than the corresponding values for D_2O adsorption, although the differences are within 3 standard deviations below $p/p^0 \sim 0.3$ (see Figure 9). In liquid H_2O, the quantum effect is mainly due to rotational uncertainty because the water molecule has small moments of inertia but a relatively large total mass.[46] Therefore, it is proposed that quantum effects, which give greater orientational uncertainty for adsorbed H_2O molecules, produce higher barriers to diffusion for H_2O compared with D_2O adsorption and differences in adsorption kinetics at low p/p^0.

High Relative Pressure ($p/p^0 > 0.4$)/Pore Filling Region. The availability of surface groups decreases with increasing adsorption and the adsorbate−adsorbate interactions in the associative mechanism become increasingly significant. Above $p/p^0 = \sim$0.4, the activation energies for H_2O adsorption are much higher than those for D_2O adsorption. The higher barriers to diffusion of H_2O into BAX950 compared with D_2O imply more marked kinetic temperature dependence for H_2O adsorption. The SE exponent (β) increases with increasing p/p^0 and approaches 1 at $p/p^0 = \sim$0.45 for both adsorbents, which have quite different functional groups characteristics and porous structures. This is the region of the isotherm in which the development and merging of H_2O/D_2O clusters occurs, eventually leading to pore filling. The structure of adsorbed H_2O and D_2O becomes significant in determining adsorption characteristics in this region. Adsorbed H_2O has a different structure and properties

compared with bulk water due to the H_2O−surface interactions and confinement in pores suppresses formation of highly directional 3-D bonds in the adsorbate.[51,52] The effects of confinement are greater for hydrophilic surfaces than for hydrophobic surfaces.[53] Also, the pore size distributions of both carbons used in this study suggest that confinement effects will be significant over the complete pressure ranges of the isotherms. Diffusivities in bulk fluids increase due to quantum tunneling and this effect is greater for H_2O than D_2O.[54] Studies of orientational dynamics of H_2O confined in hydrophobic and hydrophilic silica nanopores shows that in both types of pores the dynamics depend on the pore size and are significantly slower than in the bulk liquid.[55] The effect of confinement on H_2O diffusivity was more marked for smaller pores.

Bulk H_2O liquid is less structured than D_2O due to the weaker O····H—O bond compared with the O····D—O bond.[46] The intermolecular hydrogen bond interactions are very directional and in quantum systems they are averaged over the molecular rotational uncertainty. The larger orientational uncertainty for H_2O compared to D_2O leads to a softening of the effective intermolecular potential for H_2O relative to D_2O. The average orientational uncertainties are smaller than the estimated de Broglie wavelength for a free proton at room temperature.[46] Confinement in pores suppresses the formation of highly directional O····H—O 3-D networks in H_2O.[51] It is proposed that the effect of confinement in pores is greater for H_2O than for D_2O because the O····H—O bond is weaker than the O····D—O bond. Therefore, the disruption of the H_2O network structure should be greater than for D_2O, leading to increased structural differences compared with bulk H_2O and D_2O. The structural perturbation by confinement in pores will influence cluster formation and merger, and adsorbate structure. It is proposed that the more diffuse, less structured H_2O adsorbate compared with D_2O produces a higher barrier to diffusion for H_2O than for D_2O in pores.

Role of Specific Functional Groups. The kinetic results have been discussed in terms of hydrogen bonding of molecules to surface functional groups and associative interactions in general in the confined adsorbate phase. However, some differences might be expected for H-bonding via the H of H_2O to O surface groups and the O of H_2O to OH surface groups. Benoit et al. used a rigid-body diffusion quantum Monte Carlo method to study the ground state and energetics of phenol $(H_2O)_n$ where $n = 2-5$.[56] The results indicated that the lowest energy phenol H_2O system involved the oxygen in the H_2O bonding to the phenolic H rather than the H in H_2O bonding to the O in phenol. Also, a π-bonded structure for phenol H_2O was proposed. Titration studies indicated that the oxygen functional groups in BAX950 were mainly (78%) phenolic groups. Therefore similar interactions with phenolic surface functional groups may occur when H_2O molecules are confined in pores and differences may be expected when D_2O is adsorbed on activated carbons.

5. Conclusions

Quantum effects have a significant influence on the structures and properties of liquid H_2O and D_2O. Adsorption isotherms for H_2O and D_2O on activated carbons were very similar, but significant differences were observed for isotherm hysteresis and adsorption kinetics. These differences are related to small differences in adsorbate−adsorbent and adsorbate−adsorbate interactions and adsorbate structures for H_2O and D_2O. A kinetic isotope effect in which D_2O adsorption kinetics were faster than the corresponding H_2O kinetic parameters at 298 K was observed for both acidic and basic carbons with markedly different pore structures at low relative pressures ($p/p^0 < \sim 0.4$) in which adsorbate−adsorbent interactions are important. A detailed study of one of the carbons showed that the activation energies were lower for D_2O adsorption than H_2O over the whole uptake range investigated. These observations are consistent with quantum effects producing more orientational uncertainty for H_2O and confinement in pores having a greater effect on H_2O than D_2O adsorbate structure due the greater effect on hydrogen bond network structure because of the slightly weaker O····H—O compared with O····D—O intermolecular bonding. These effects influence cluster formation and adsorbate structure, giving lower activation energies for diffusion of D_2O into the porous structure compared with H_2O. This kinetic isotope effect is quite different from the observation of a kinetic isotope quantum molecular sieving effect for H_2 and D_2 in which the higher zero-point energy of the former gives rise to a higher barrier to diffusion when the difference in the adsorbate molecule and pore sizes is close to the de Broglie wavelength, leading to slower adsorption kinetics for H_2 compared with D_2. It represents the first observation of a kinetic isotope quantum effect for diffusion into porous materials related to adsorbate−adsorbent surface chemistry and the effect of confinement on adsorbate−adsorbate interactions.

Supporting Information Available: TPD studies, kinetic profiles, and Arrhenius graphs are given. This material is available free of charge via the Internet at http://pubs.acs.org.

References and Notes

(1) Fletcher, A. J.; Benham, M. J.; Thomas, K. M. *J. Phys. Chem. B* **2002**, *106*, 7474.
(2) Muller, E. A.; Rull, L. F.; Rega, L. F.; Gubbins, K. E. *J. Phys. Chem.* **1996**, *100*, 1189.
(3) Nemethy, G.; Scheraga, H. A. *J. Chem. Phys.* **1964**, *41*, 680.
(4) Frank, H. S. In *Water: A Comprehensive Treatise;* Franks, F., Ed.; Plenum: New York, 1972; Vol. 1; pp 515−542.
(5) Shroto, H.; Pal, H.; Tominga, K.; Yoshimara, K. *J. Phys. Chem.* **1996**, *100*, 14575.
(6) Owtrusky, J. C.; Baronavski, A. P. *Chem. Phys.* **1998**, *110*, 11206.
(7) Forsythe, K. M.; Makri, N. *J. Chem. Phys.* **1999**, *110*, 6082.
(8) Szabo, Z. *Inorg. Chem.* **1998**, *37*, 6214.
(9) Stutz, J.; Ezell, M. J.; Finlayson-Pitts, B. J. *J. Phys. Chem. A* **1997**, *101*, 9187.
(10) Yussouff, M.; Rao, B. K.; Jena, P. *Solid State Commun.* **1995**, *94*.
(11) Pyun, S.-I.; Lim, C.; Kim, K.-B. *J. Alloys Compd.* **1994**, *203*, 149.
(12) Herro, D.; Hirschler, M. M. *Owid. Commun.* **1984**, *7*, 321.
(13) Zhao, X.; Villar-Rodil, S.; Fletcher, A. J.; Thomas, K. M. *J. Phys. Chem. B* **2006**, *110*, 9947.
(14) Boehm, H. P. *Carbon* **1994**, *32*, 759.
(15) Benham, M. J.; Ross, D. K. *Z. Phys. Chem. (Neue Folge)* **1989**, *163*, 25.
(16) *Lange's Handbook of Chemistry*, 15th ed.; McGraw-Hill: New York, 1999.
(17) Dubinin, M. M.; Radushkevich, L. V. *Proc. Acad. Sci. USSR* **1947**, *55*, 331.
(18) Cazorla-Amoros, D.; Alcaniz-Monge, J.; de le Casa-Lillo, M. A.; Linares-Solano, A. *Langmuir* **1998**, *14*, 4589.
(19) Cazorla-Amoros, D.; Alcaniz-Monge, J.; Linares-Solano, A. *Langmuir* **1996**, *12*, 2820.
(20) Linares-Solano, A.; Salinas Martínez de Lecea, C.; Monge, J. A.; Cazorla-Amorós, D. *Tanso* **1998**, *185*, 316.
(21) Barrett, E. P.; Joyner, L. G.; Halenda, P. P. *J. Phys. Chem.* **1951**, *73*, 373.
(22) Dubinin, M. M.; Stoeckli, H. F. *J. Coll. Interf. Sci.* **1980**, *75*, 34.
(23) Xiao, B.; Boudou, J. P.; Thomas, K. M. *Langmuir* **2005**, *21*, 3400.
(24) Harding, A. W.; Foley, N. J.; Norman, P. R.; Francis, D. C.; Thomas, K. M. *Langmuir* **1998**, *14*, 3858.
(25) Sing, K. S. W.; Everett, D. H.; Haul, R. A. W.; Moscou, L.; Pierotti, R. A.; Rouquerol, J.; Siemieniewska, T. *Pure Appl. Chem.* **1985**, *57*, 603.
(26) Laidler, K. J. *Chemical Kinetics*, 3rd ed.; Harper and Row: New York, 1987.
(27) Chagger, H. K.; Ndaji, F. E.; Sykes, M. L.; Thomas, K. M. *Carbon* **1995**, *33*, 1405.

(28) O'Koye, I. P.; Benham, M.; Thomas, K. M. *Langmuir* **1997**, *13*, 4054.
(29) Reid, C. R.; O'Koye, I. P.; Thomas, K. M. *Langmuir* **1998**, *14*, 2415.
(30) Reid, C. R.; Thomas, K. M. *Langmuir* **1999**, *15*, 3206.
(31) Reid, C. R.; Thomas, K. M. *J. Phys. Chem. B* **2001**, *105*, 10619.
(32) Shlesinger, M. F.; Montroll, E. W. *Proc. Natl. Acad. Sci.* **1984**, *81*, 1280.
(33) Klafter, J.; Shlesinger, M. F. *Proc. Natl. Acad. Sci.* **1986**, *83*, 848.
(34) Fletcher, A. J.; Thomas, K. M. *Langmuir* **2000**, *16*, 6253.
(35) Fletcher, A. J.; Thomas, K. M. *Langmuir* **1999**, *15*, 6908.
(36) Arnell, J. C.; McDermott, H. L. *Can. J. Chem.* **1952**, *30*, 177.
(37) Berenguer-Murcia, A.; Fletcher, A. J.; Garcia-Martinez, J.; Cazorla-Amoros, D.; Linares-Solano, A.; Thomas, K. M. *J. Phys. Chem. B* **2003**, *107*, 1012.
(38) Freeman, J. J.; Tomlinson, J. B.; Sing, K. S. W.; Theocharis, C. R. *Carbon* **1993**, *31*, 865.
(39) Freeman, J. J.; Tomlinson, J. B.; Sing, K. S. W.; Theocharis, C. R. *Carbon* **1995**, *32*, 795.
(40) Fletcher, A. J.; Cussen, E. J.; Prior, T. J.; Rosseinsky, M. J.; Kepert, C. J.; Thomas, K. M. *J. Am. Chem. Soc.* **2001**, *123*, 10001.
(41) Fletcher, A. J.; Cussen, E. J.; Bradshaw, D.; Rosseinsky, M. J.; Thomas, K. M. *J. Am. Chem. Soc.* **2004**, *126*, 9750.
(42) Hirschfelder, J. O.; Curtiss, C. F.; Bird, R. B. *Molecular Theory of Gases and Liquids*; Wiley: New York, 1966.
(43) Kumar, A. V. A.; Bhatia, S. K. *Phys. Rev. Lett.* **2005**, *95*, 245901.
(44) Kumar, A. V. A.; Jobic, H.; Bhatia, S. K. *J. Phys. Chem. B* **2006**, *110(33)*, 16666.
(45) Webster, C. E.; Drago, R. S.; Zerner, M. C. *J. Am. Chem. Soc.* **1998**, *120*, 5509.
(46) Hernandez de la Pena, L.; Kusalik, P. G. *J. Chem. Phys.* **2004**, *121*, 2992.
(47) Hernandez de la Pena, L.; Gulam Razul, M. S.; Kusalik, P. G. *J. Phys. Chem. A* **2005**, *109*, 7236.
(48) Hernandez de la Pena, L.; Gulam Razul, M. S.; Kusalik, P. G. *J. Chem. Phys.* **2005**, *123*, 144506.
(49) Hernandez de la Pena, L.; Kusalik, P. G. *J. Am. Chem. Soc.* **2005**, *127*, 5246.
(50) Crabtree, A.; Siman-Tov, M. *Thermophysical properties of saturated light and heavy water for advanced neutron source applications*; Oak Ridge National Laboratory: Oak Ridge, Tennessee, 1993; Vol. ORNL/TM-12322.
(51) Raviv, U.; Laurat, P.; Klein, J. *Nature* **2001**, *413*, 51.
(52) Raviv, U.; Laurat, P.; Klein, J. *J. Chem. Phys.* **2004**, *116*, 5167.
(53) Yamaguchi, T.; H, H. H.; Kittaka, S. *J. Mol. Liq.* **2006**, *129*, 57.
(54) Guillot, B.; Guissani, Y. *J. Chem. Phys.* **1998**, *108*, 10162.
(55) Scodinu, A.; Fourkas, J. T. *J. Phys. Chem. B* **2002**, *106*, 10292.
(56) Benoit, D. M.; Clary, D. C. *J. Phys. Chem. A* **2000**, *104*, 5590.